Cell Reports, Volume *34*

Supplemental Information

Impact of WIN site inhibitor on the WDR5 interactome

Alissa D. Guarnaccia, Kristie L. Rose, Jing Wang, Bin Zhao, Tessa M. Popay, Christina E. Wang, Kiana Guerrazzi, Salisha Hill, Chase M. Woodley, Tyler J. Hansen, Shelly L. Lorey, J. Grace Shaw, William G. Payne, April M. Weissmiller, Edward T. Olejniczak, Stephen W. Fesik, Qi Liu, and William P. Tansey

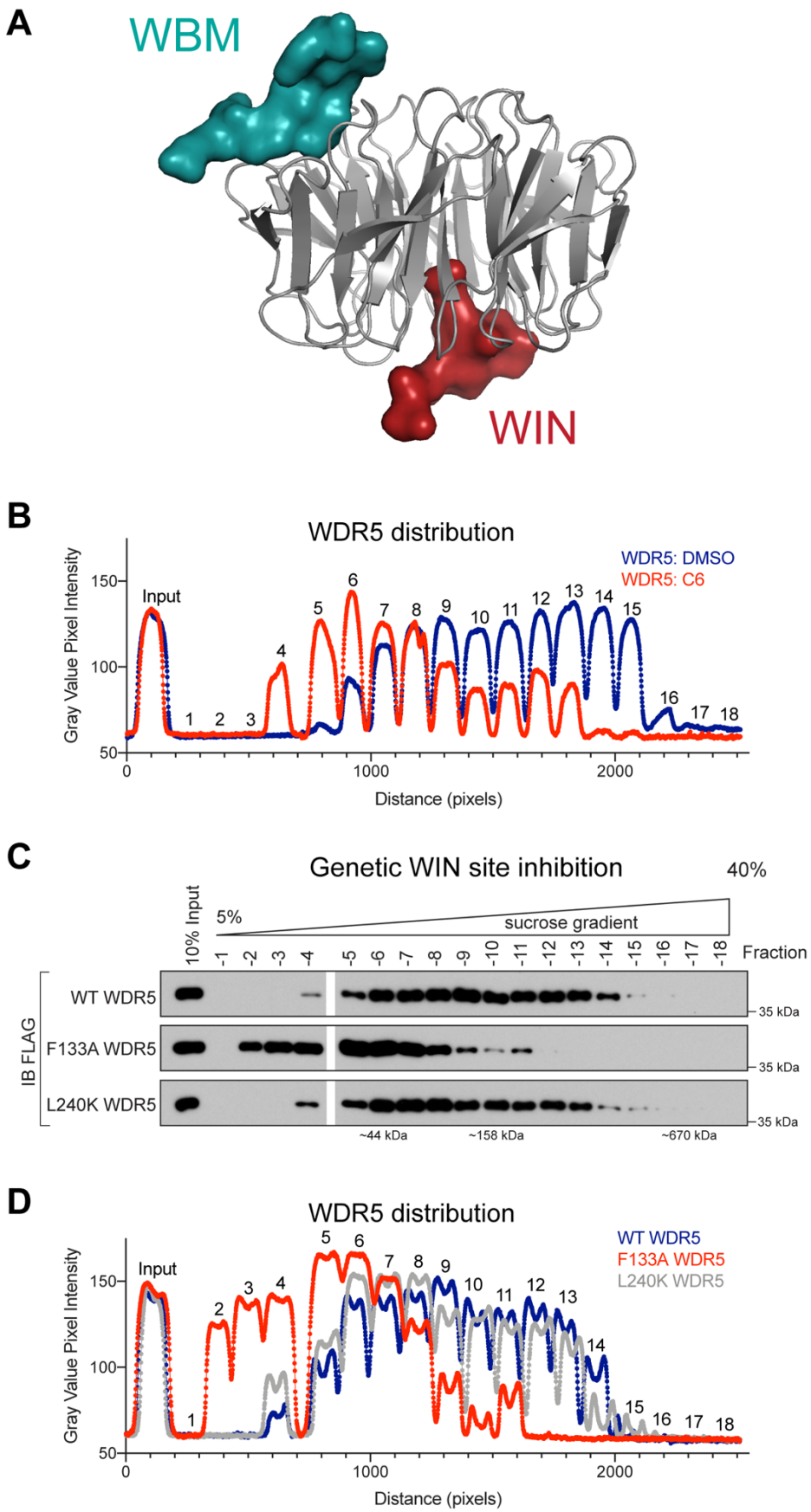

Figure S1: Analysis of WDR5 complexes and interacting proteins. Related to Figure 1. (**A**) Co-crystal structure of WDR5 (grey) with KMT2A peptide (red) bound at the WIN site and RBBP5 peptide (teal) bound at the WBM site (PDB: 3P4F). (**B**) Graphical representation of the WDR5 data from **Figure 1B** as plot profiles that graph the intensities for each pixel across the IB images. (**C**) Density sedimentation analysis of HEK293 extracts from cells stably expressing FLAG-tagged WDR5; wild-type (WT) or the F133A or L240K mutants.

Immunoblots (IB) were probed with an anti-FLAG antibody. Positions of molecular weight markers are indicated. *n=3* biological replicates. (**D**) Graphical representation of the data from Figure S1C as plot profiles that graph the intensities for each pixel across the IB images.

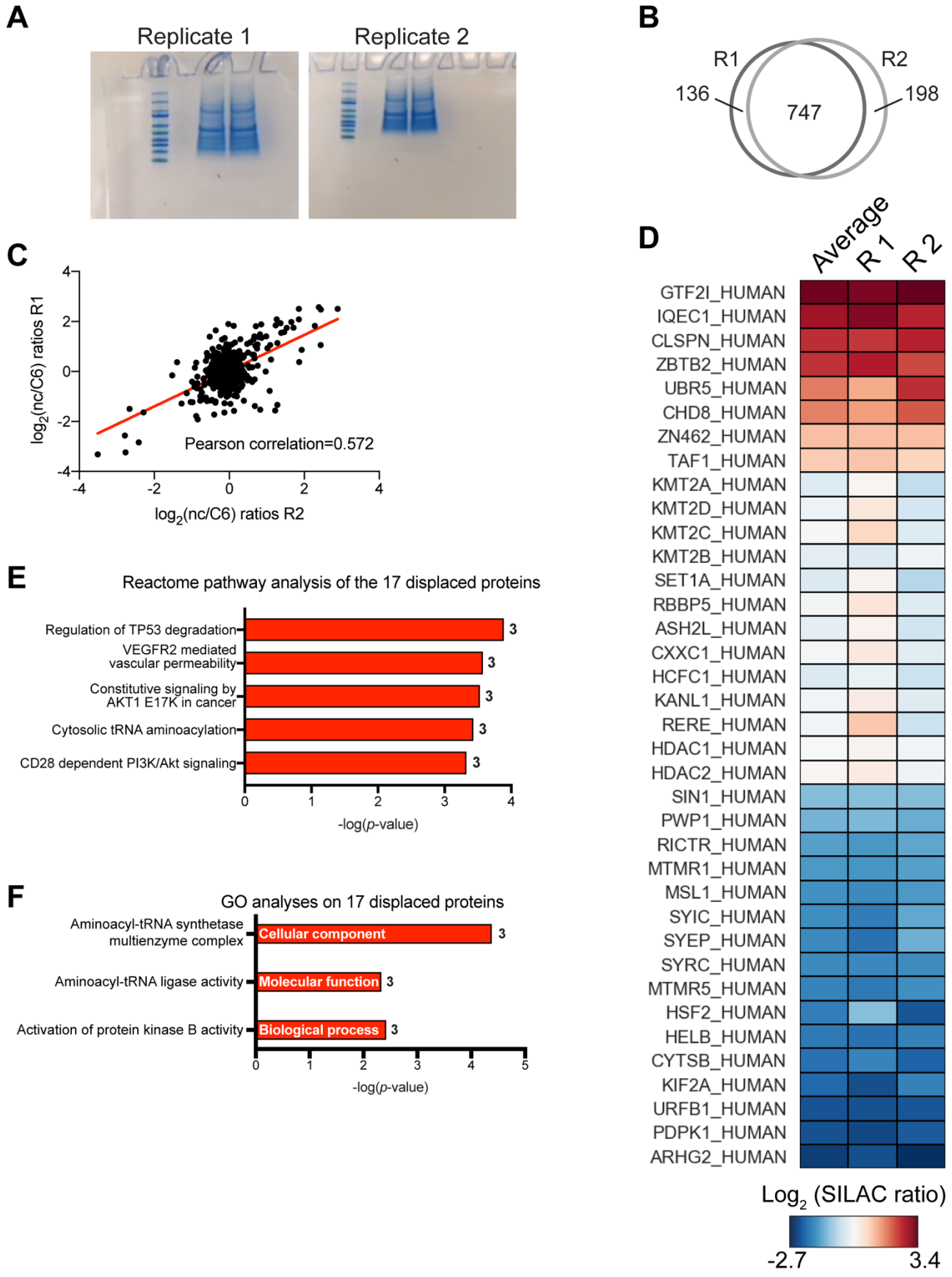

Figure S2: Quantitative proteomic analysis of the impact of C6 on the WDR5 interactome. Related to Figure 2. (**A**) SILAC samples for mass spectrometry. Short stack Coomassie-stained gels of FLAG-WDR5 IP samples prior to trypsin digestion and LC MS/MS. Heavy and Light samples were pooled before loading in two lanes of each gel. (**B**) Venn diagram of the overlap between replicates. (**C**) Comparison of SILAC duplicate

experiments. Pearson correlation coefficient was calculated with Perseus software. (**D**) Heatmap of the subset of proteins represented in Figure 2D. (**E**) Reactome pathways analysis of the 17 proteins that are displaced from WDR5 in the presence of C6. These proteins were analyzed using PANTHER Overrepresentation Test with the “Reactome pathways” Annotation Data Set (Reactome version 65 Released 2019-12-22). The five enriched categories are shown; numbers on the right are the number of proteins in each category. (**F**) Gene ontology analysis of the 17 displaced proteins. These proteins were analyzing using PANTHER Overrepresentation Tests with “GO biological function complete,” “GO molecular function complete,” and “GO cellular compartment complete" Annotation Data Sets. Only one category was enriched for each of these Annotation Data Sets and each of these categories is described in the graph with the number of proteins in each category listed on the right.

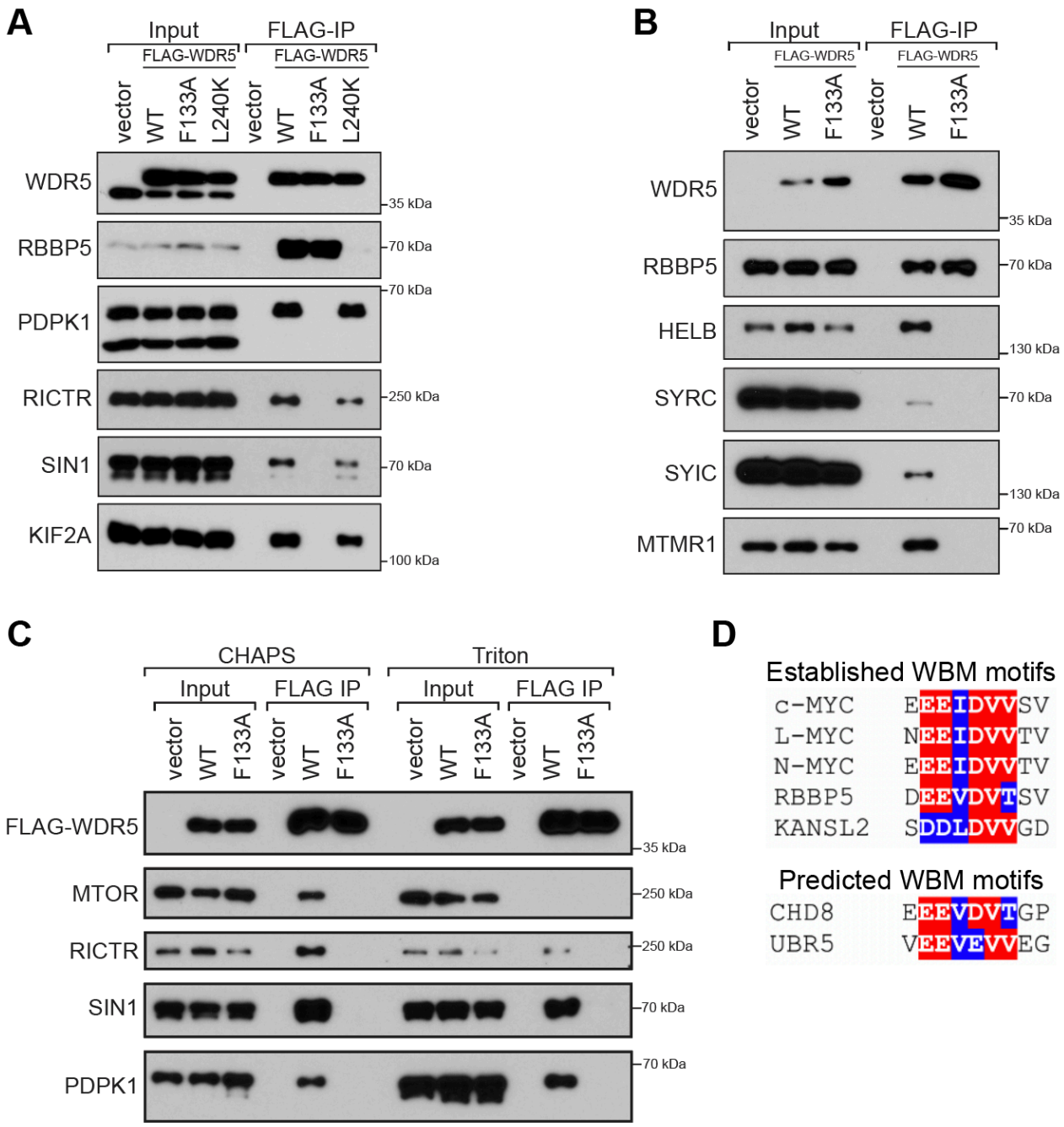

Figure S3: Mutation of the WIN site affects protein interactions with WDR5. Related to Figure 3. (**A**) Genetic validation of WIN site-dependent WDR5 binding proteins identified by SILAC. Immunoblots of coIP experiments from HEK293 cells stably expressing FLAG-tagged WDR5 variants. Inputs are 20% for WDR5 and 10% for others; *n=3* biological replicates. The antibody used for PDPK1 is Bethyl A302-130A. (**B**) As in (A) but for a second set of WDR5-interacting proteins. Inputs are 10% for WDR5 and RBBP5 and 1% for others. *n=3* biological replicates. (**C**) mTORC2 components can bind WDR5 in the presence of CHAPS but not Triton X-100. Lysates from HEK293 cells stably expressing FLAG-tagged WDR5 proteins were prepared in buffer containing either CHAPS or Triton X-100 and subject to FLAG IP under those same conditions. IP samples were probed with antibodies against the indicated proteins. Inputs are 10% for WDR5 and 1% for all others; *n=3* biological replicates. (**D**) Comparison of established WBM motifs to predicted WBM motifs in CHD8 and UBR5.

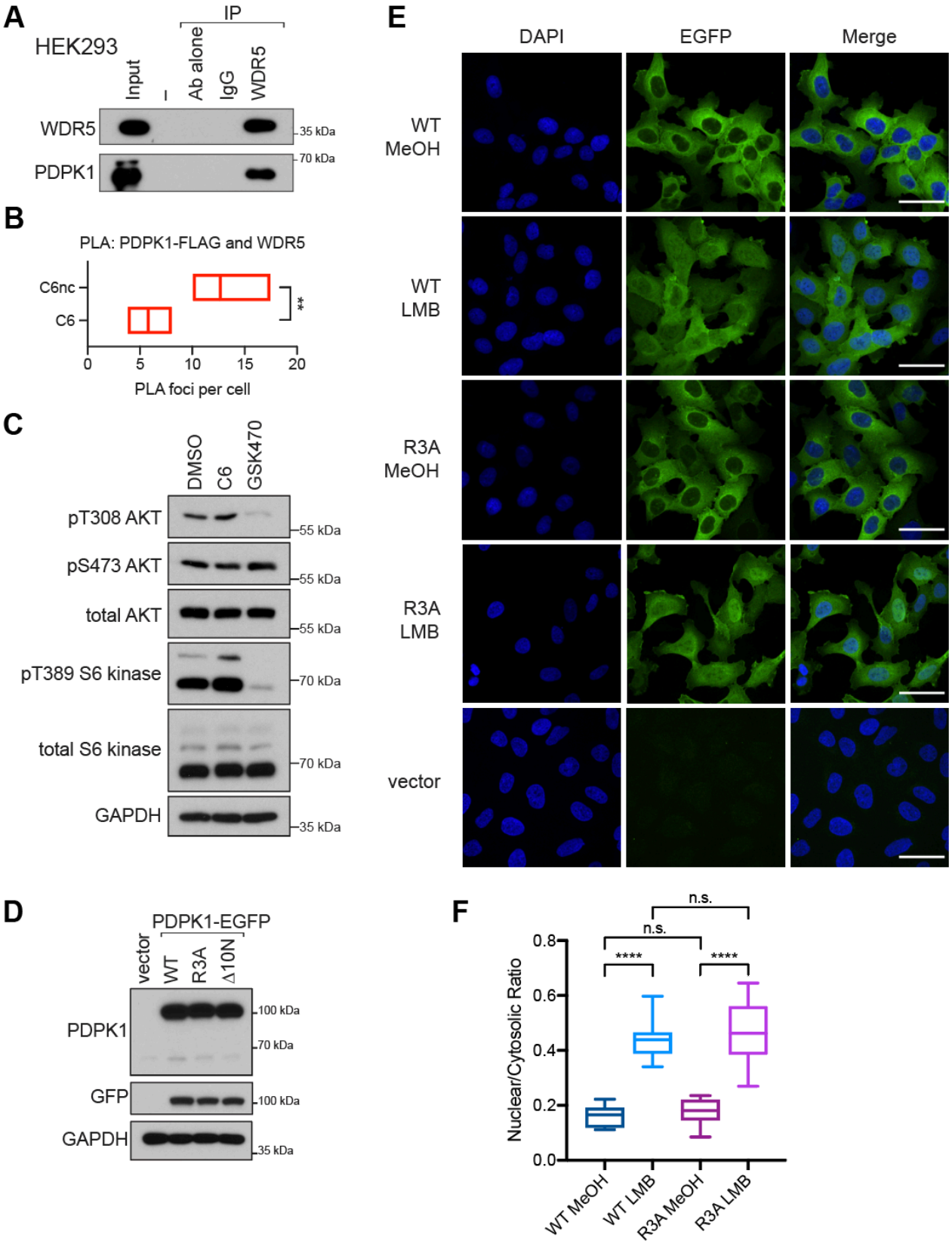

Figure S4: The PDPK1–WDR5 interaction does not influence PDPK1 signaling or nuclear shuttling. Related to Figure 4. (**A**) Reciprocal coimmunoprecipitation between endogenous WDR5 and PDPK1; performed in HEK293 cells. Input is 5% for WDR5 and 1% for PDPK1. *n=3* biological replicates. (**B**) Quantification of proximity ligation assay between PDPK1–FLAG and WDR5 shown in Figure 4B. Quantification of foci per cell with line representing the mean, and bars representing the min and max; *n=3*, unpaired two-tailed *t*-test, $^{**}p = 0.0037$. (**C**) C6 WIN site inhibition has little if any effect on AKT signaling in CHP134 cells. Cells were treated overnight with 5 μM C6, 2 μM PDPK1 kinase inhibitor GSK2334470, or

DMSO vehicle control. Cells were then treated with 50 ng/ml IGF-1 for 30 minutes before lysis in RIPA buffer supplemented phosphatase inhibitors. Lysates were analyzed by western blotting. *n=3* biological replicates. (**D**) Overexpression of PDPK1-EGFP fusion proteins. U2OS cells were stably transduced with pBabe-puro vectors to express PDPK1-EGFP-FLAG fusion proteins: wildtype, R3A mutant, or deletion mutant without the first ten amino acids, Δ10. (**E**) Representative images from the experiments quantified in (D). Immunofluorescence of the indicated stable cell lines treated for four hours either with 70% methanol vehicle control or with 20 nM leptomycin B. Cells were then fixed, mounted in DAPI-containing media, and imaged. Scale bar is 50 μm. (**F**) PDPK1 shuttling capability is not affected by disrupting the interaction with WDR5. Quantification of the nuclear localization of WT and R3A PDPK1 when nuclear export is inhibited by four-hour treatment with 20 nM leptomycin B (LMB) or 70% methanol vehicle control. Plotted as box and whisker plot where the line is at the median, the box represents 25th to 75th percentiles, and whiskers represent min and max; *n=3*, analyzed by unpaired two-tailed *t*-test, **** $p < 0.0001$.

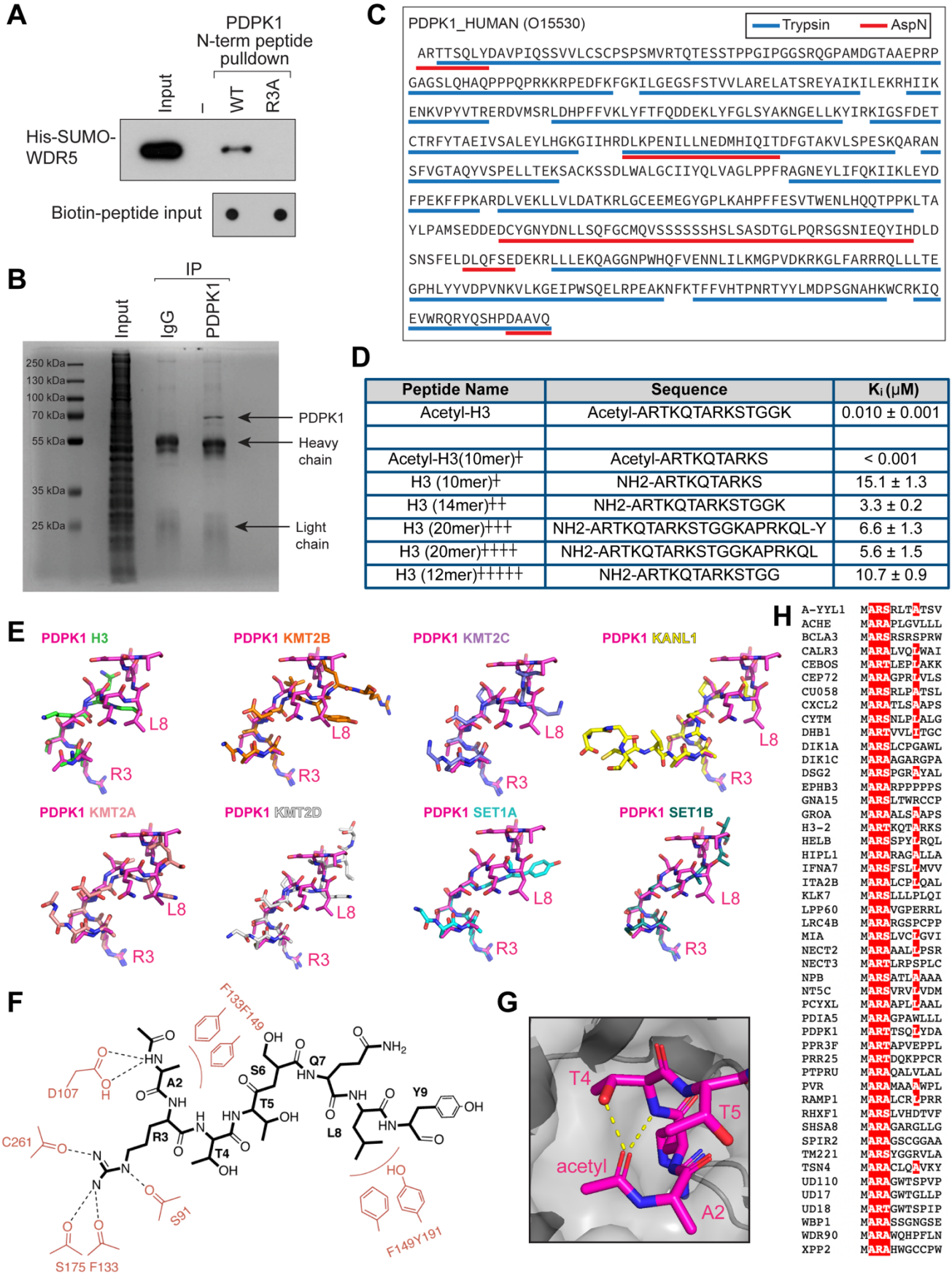

Figure S5: The N-terminus of PDPK1 is acetylated and binds to the WIN site of WDR5. Related to Figure 5. (A) Biotinylated peptides were pre-bound to streptavidin beads and incubated with recombinant 6xHis-SUMO-WDR5. Recovery of WDR5 was analyzed by IB. PDPK1 peptides do not include Met1 and are not acetylated. (**B**) Purification of PDPK1 for MS/MS analysis of post-translational modifications. Coomassie-stained gel of endogenous PDPK1 purified by IP from HEK293 cells. Top arrow denotes the PDPK1 band that

was cut out and taken forward for analysis. Co-purified immunoglobulin heavy and light chains are indicated. (**C**) PDPK1 sequence coverage by tandem mass spectrometry for trypsin and for AspN cleavages. Coverage with trypsin (75%) is shown as blue underline, and coverage with AspN (15%) is shown as red underline. Although trypsin had high sequence coverage, only AspN had N-terminal coverage. (**D**) TR-FRET analysis of acetyl-H3 compared to published affinity values for histone H3 peptides. For the TR-FRET measurement the peptide is amidated at the C terminus; two or more repeats were obtained and average K_i values and standard deviations are reported. Published binding constants: +measured by fluorescence polarization (Karatas et al., 2010); ++measured by SPR (Ruthenburg et al., 2006); +++measured by ITC (Couture et al., 2006); ++++ measured by SPR (Migliori et al., 2012); +++++ measured by ITC (Lorton et al., 2020). (**E**) PDPK1 interacts with WDR5 in a manner similar to other WIN motifs. The figures show superimposition of the PDPK1 (magenta, PDB: 6WJQ) with published WIN motif co-crystal structures: unmodified histone H3 (green, PDB: 2H9M), KMT2B (orange, PDB: 3UVM), KMT2C (lavender, PDB: 3UVL), KANL1 (yellow, PDB: 4CY2), KMT2A (rose, PDB: 3EG6), KMT2D (white, PDB: 3UVK), SET1A (cyan, PDB: 3UVN), and SET1B (teal, PDB: 3UVO). (**F**) Summary of residue interactions between WDR5 and the PDPK1 WIN peptide. The PDPK1 peptide is in black and critical WDR5 residues are in red. Hydrophobic contacts are shown as red arcs and polar contacts are shown as black dotted lines. (**G**) Intramolecular hydrogen bonding stabilizes the WDR5-acPDPK1 interaction. Co-crystal structure of WDR5 in complex with acetylated PDPK1 peptide shows hydrogen bonding between carboxyl group of the acetyl group and T4 which stabilizes the conformation of the peptide. WDR5 is grey and PDPK1 is pink. Yellow dotted lines denote hydrogen bonds. (**H**) Analysis comparing the potential N-terminal WIN motifs (defined A/R/AST) to the consensus WIN motif sequence defined in Figure 5H. Residues that match the consensus are highlighted in red. Only one H3 variant is listed because all variants are identical. A-YYL1 is an abbreviation for A0A0A6YYL1.

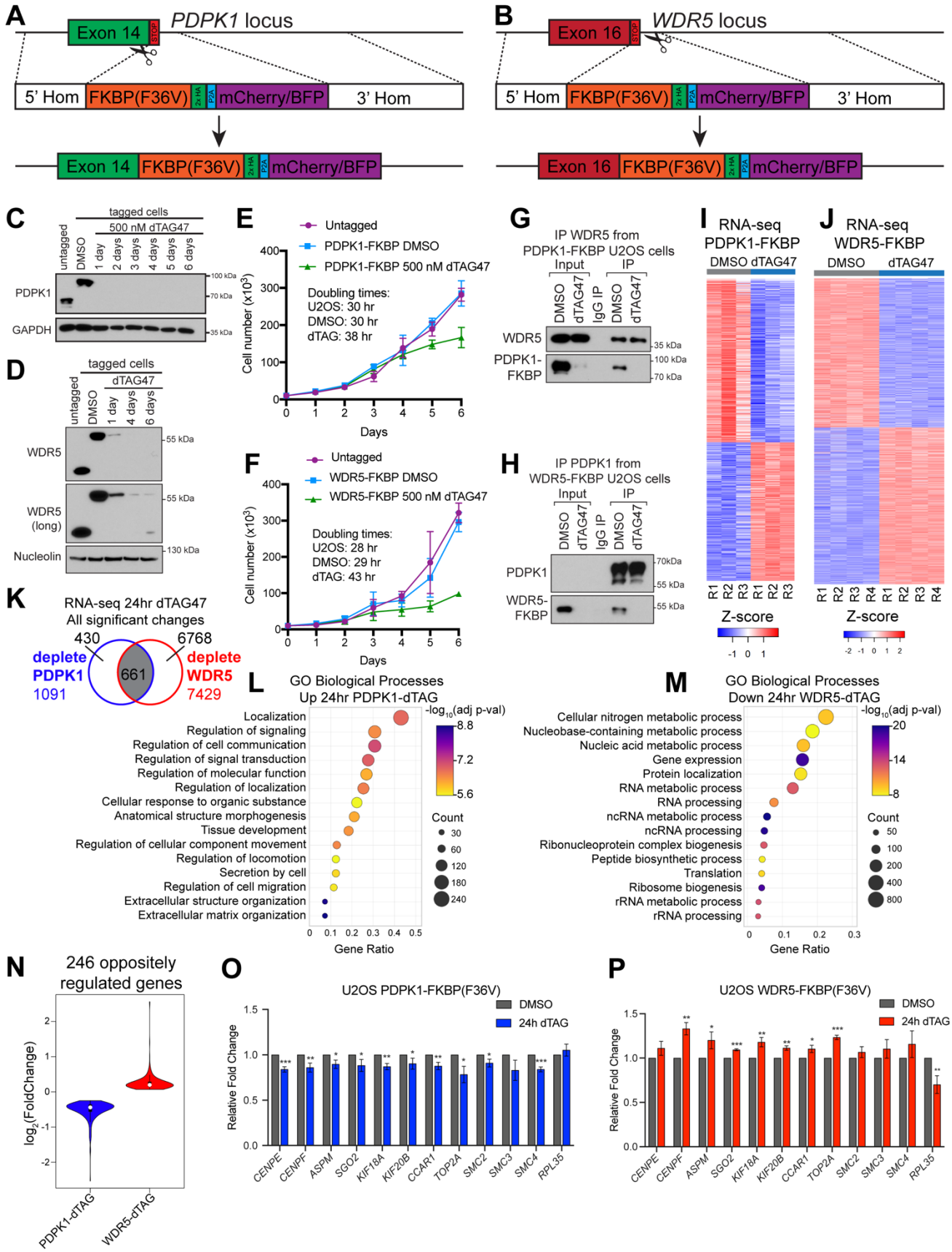

Figure S6: Inducible degradation of PDPK1 and WDR5 enables comparative genomic analysis. Related to Figure 6. (**A**) Schematic of the CRISPR targeting strategy used to tag endogenous PDPK1 for degradation. Cassettes containing FKBP(F36V)-2xHA-P2A-mCherry (or BFP) were introduced near the stop codon of PDPK1. A population of cells was isolated by fluorescence activated cell sorting using the mCherry and BFP markers. (**B**) Schematic of the CRISPR targeting strategy used to tag endogenous WDR5 for degradation.

Cassettes containing FKBP(F36V)-2xHA-P2A-mCherry (or BFP) were introduced near the stop codon of WDR5. A population of cells was isolated by fluorescence activated cell sorting using the mCherry and BFP markers. (**C**) IB, showing that tagged PDPK1 results in a shift in the apparent molecular weight of the protein, and that knock down by addition of 500 nM dTAG47 is stable for at least six days. (**D**) IB, showing that tagged WDR5 results in a shift in the apparent molecular weight of the protein, and that knock down by addition of 500 nM dTAG47 is stable for at least six days. Note that, by day 6, untagged WDR5 becomes visible in IB (long exposure), which reflects an outgrowth of cells with untagged *WDR5* loci in the population. (**E**) Analysis of cell growth of PDPK1-FKBP(F36V)-2xHA cells. Cells were counted every 24 hours, error bars represent standard deviation, *n=3*. The doubling time for a representative experiment is shown. (**F**) Analysis of cell growth of WDR5-FKBP(F36V)-2xHA cells. Cells were counted every 24 hours, error bars represent standard deviation, *n=3*. The doubling time for a representative experiment is shown. The apparent survival of WDR5-depleted cells at day 6 is due to outgrowth of cells with untagged *WDR5* loci in the population. (**G**) The PDPK1–WDR5 interaction is preserved in PDPK1-FKBP(F36V)-2xHA cells. CoIP of endogenous proteins from PDPK1-FKBP(F36V)-2xHA cells. Input for WDR5 is 10%. Input for PDPK1 is 1%. *n=3* biological replicates. (**H**) The PDPK1–WDR5 interaction is preserved in WDR5-FKBP(F36V)-2xHA cells. CoIP of endogenous proteins from WDR5-FKBP(F36V)-2xHA cells. Input for PDPK1 is 10%. Input for WDR5 is 1%. *n=3* biological replicates. (**I**) Heatmap, displaying z-transformed gene expression for significantly changed genes in 24 hr dTAG47 versus DMSO (FDR < 0.05) for three replicates (R1–R3) of RNA-Seq from PDPK1-FKBP(F36V)-2xHA U2OS cells. (**J**) Heatmap, displaying z-transformed gene expression for significantly changed genes in 24 hr dTAG47 versus DMSO (FDR < 0.05) for four replicates (R1–R4) of RNA-Seq from WDR5-FKBP(F36V)-2xHA U2OS cells. (**K**) Venn diagram of overlap of significantly changed genes between RNA-Seq from WDR5 depletion and PDPK1 depletion datasets. (**L**) GO term analysis of increased transcripts identified by RNA-Seq of U2OS cells depleted of PDPK1 for 24 hours. Biological Process GO terms were ranked by adjusted *p*-value, and the 15 most significant enriched terms are presented; the color indicates the Bonferroni-corrected Fisher Exact *p*-value; the size indicates the number of genes in that category; the x axis the ratio of genes in the category over total analyzed genes. (**M**) GO term analysis of decreased transcripts identified by RNA-Seq of U2OS cells depleted of WDR5 for 24 hours. Ranking and presentation are as in (L). (**N**) Violin plot of the 246 gene expression changes that are decreased with PDPK1 depletion and increased with WDR5 depletion. (**O**) Gene expression analysis by RT-qPCR to validate PDPK1 depletion RNA-Seq results. U2OS PDPK1-FKBP(F36V)-2xHA cells were treated for 24 hours with 500 nM dTAG47 or DMSO vehicle control, RNA collected, reverse transcribed, and analyzed by qPCR. Signal is normalized to *GAPDH*. Error bars represent standard deviation, *n=3* independent biological replicates. *** $p<0.001$, ** $p<0.01$, * $p<0.05$ by unpaired two-tailed *t*-test. (**P**) Gene expression analysis by RT-qPCR to validate WDR5 depletion RNA-Seq results. U2OS WDR5-FKBP(F36V)-2xHA cells were treated for 24 hours with 500 nM dTAG47 or DMSO vehicle control, RNA collected, reverse transcribed, and analyzed by qPCR. Signal is normalized to *RPL14*. Error bars represent standard deviation, *n=3* independent biological replicates. *** $p<0.001$, ** $p<0.01$, * $p<0.05$ by unpaired two-tailed *t*-test.

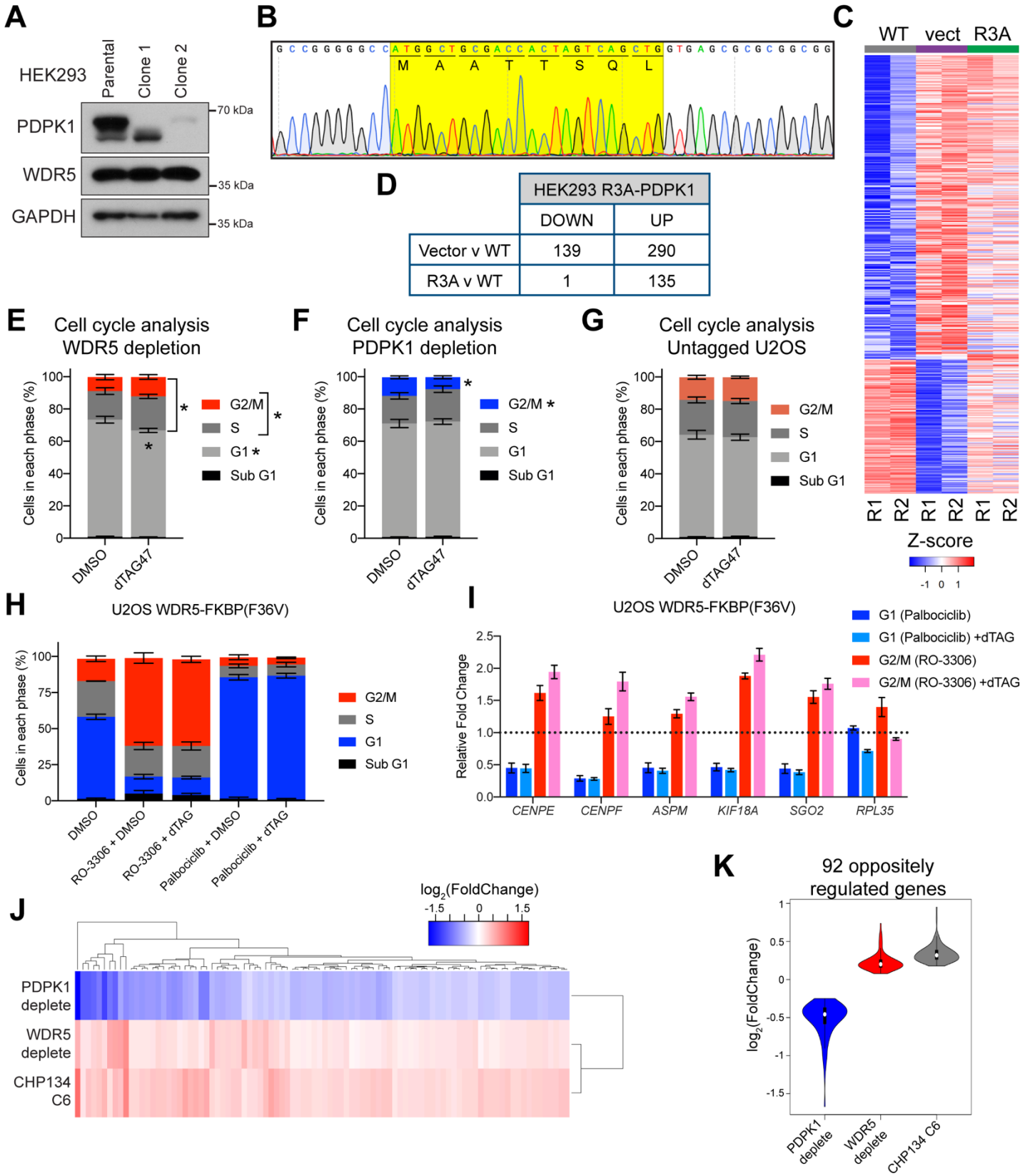

Figure S7: Disrupting the PDPK1–WDR5 interaction causes increased gene expression of cell cycle genes. Related to Figure 7. (**A**) HEK293 cells were engineered with CRISPR/Cas9 and a single stranded template to express only the R3A mutant of PDPK1. IB analysis of two clones compared to unedited cells is shown, demonstrating a lower level of expression. Clone 2 was taken forward for retroviral add-back of PDPK1 variants and analysis by RNA-Seq. (**B**) Chromatogram of Sanger sequencing of genomic DNA from Clone 2 in (A). Yellow highlights the sequence of the first coding intron of PDPK1 and demonstrates efficient integration of the R3A mutation. DNA sequence is at the top, and black letters below indicate the protein sequence. (**C**) Heatmap displaying z-transformed gene expression measured by RNA-Seq from the R3A-engineered HEK293

cells. The 429 significantly changed (FDR < 0.05) genes are compared for WT PDPK1 overexpression, low R3A PDPK1 expression (vector), and R3A PDPK1 overexpression in two replicates. (**D**) Results of RNA-Seq in HEK293 cells to assess the consequences of the PDPK1 R3A mutant. Table shows the number of transcripts significantly (FDR < 0.05) altered with low (vector) and high R3A PDPK1 expression, compared high WT PDPK1 expression. *n=2* biological replicates for each condition. (**E**) Distribution of cell cycle phases as determined by flow cytometry for WDR5-FKBP(F36V)-2xHA U2OS cells treated for 24 hours with 500 nM dTAG47or DMSO vehicle control. Data are presented as mean and error bars are SEM; * $p < 0.05$ by unpaired two-tailed *t*-test. *n=4* biological replicates. (**F**) Distribution of cell cycle phases as determined by flow cytometry for PDPK1-FKBP(F36V)-2xHA U2OS cells treated for 24 hours with 500 nM dTAG47 or DMSO vehicle control. Data are presented as mean and error bars are SEM; * $p = 0.016$ by unpaired two-tailed *t*-test. *n=4* biological replicates. (**G**) Distribution of cell cycle phases as determined by flow cytometry for untagged U2OS cells treated with 500 nM dTAG47 or DMSO vehicle control for 24 hours. Data are presented as mean and error bars are SEM; *n=3* biological replicates. No significance by unpaired two-tailed *t*-test. (**H**) Distribution of cell cycle phases as determined by flow cytometry for WDR5-FKBP(F36V)-2xHA U2OS cells treated for 20 hours with DMSO vehicle control, 1 μM Palbociclib (CDK2/4 inhibitor), 10 μM RO-3306 (CDK1 inhibitor), and 500 nM dTAG47 as indicated. Data are represented as mean ± SEM. *n=3* biological replicates, except for Palbociclib samples where *n=2*. (**I**) Gene expression changes are specific to cells in G2/M cell cycle phase. Gene expression analysis by RT-qPCR in U2OS WDR5-FKBP(F36V)-2xHA cells treated for 20 hours with DMSO vehicle control, 1 μM Palbociclib CDK2/4 inhibitor for G1 enrichment, 10 μM RO-3306 CDK1 inhibitor for G2/M enrichment, and 500 nM dTAG47 as indicated. Signal is normalized to *GAPDH*. Data are represented as mean ± SEM; *n=3* biological replicates. (**J**) Hierarchical clustering of $\log_2$(fold change) in gene expression over the 92 genes oppositely regulated in the U2OS data and those increased by 24-hour treatment of CHP134 cells with 5 μM C6 (GEO: GSE136451). (**K**) Violin plots compare the distribution of fold change values for the oppositely regulated genes shown in (J).

Table S2: Summary statistics of key proteins identified in WDR5 SILAC experiment. Related to Figure 2. Replicate values are reported with the slash, represented as R1 / R2.

Protein Name	Total Spectra	Razor + Unique peptides	Molecular Weight (kDa)	Sequence Coverage(%)	Ratio nc/C6 (normalized)	UniProt Accession	Official Gene Symbol
ARHG2_HUMAN	158 / 147	42 / 49	111.5	44 / 58	5.68 / 7.43	Q92974	*ARHGEF2*
KIF2A_HUMAN	82 / 56	30 / 30	79.9	44 / 55	5.67 / 3.62	O00139	*KIF2A*
PDPK1_HUMAN	52 / 39	13 / 13	63.2	28 / 30	5.95 / 5.23	O15530	*PDPK1*
PWP1_HUMAN	32 / 50	5 / 15	55.8	25 / 37	2.2 / 2.43	Q13610	*PWP1*
URFB1_HUMAN	25 / 37	22 / 26	159.5	17 / 24	5.56 / 5.44	Q6BDS2	*UHRF1BP1*
MTMR5_HUMAN	44 / 19	22 / 15	208.3	17 / 12	3.93 / 3.15	O95248	*SBF1*
HELB_HUMAN	21 / 19	16 / 12	123.2	16 / 15	4.23 / 3.62	Q8NG08	*HELB*
CYTSB_HUMAN	14 / 16	9 / 10	118.6	11 / 12	3.54 / 4.86	Q5M775	*SPECC1*
ZC21A_HUMAN	15 / 14	8 / 7	35.1	23 / 21	3.58 / 2.35	Q96GY0	*ZC2HC1A*
SYEP_HUMAN	11 / 17	9 / 14	170.6	7 / 12	4.23 / 2.40	P07814	*EPRS*
SYIC_HUMAN	13 / 13	5 / 8	144.5	4 / 7	3.80 / 2.58	P41252	*IARS*
RICTR_HUMAN	8 / 13	8 / 10	192.2	6 / 8	2.92 / 2.61	Q6R327	*RICTOR*
MSL1_HUMAN	8 / 7	4 / 4	67.1	11 / 11	3.35 / 2.89	Q68DK7	*MSL1*
HSF2_HUMAN	5 / 5	7 / 5	60.3	11 / 9	2.08 / 5.42	Q03933	*HSF2*
SIN1_HUMAN	5 / 3	4 / 2	59.1	8 / 5	2.08 / 2.13	Q9BPZ7	*MAPKAP1*
SYRC_HUMAN	6 / 2	5 / 2	75.4	9 / 3	3.37 / 3.28	P54136	*RARS*
MTMR1_HUMAN	3 / 5	2 / 4	74.7	4 / 9	2.99 / 2.76	Q13613	*MTMR1*
GTF2I_HUMAN	342 / 281	46 / 53	112.4	46 / 58	0.10 / 0.09	P78347	*GTF2I*
CHD8_HUMAN	75 / 86	31 / 37	290.5	15 / 19	0.32 / 0.20	Q9HCK8	*CHD8*
UBR5_HUMAN	60 / 98	29 / 57	309.3	14 / 28	0.35 / 0.16	O95071	*UBR5*
IQEC1_HUMAN	23 / 22	18 / 12	108.3	22 / 16	0.11 / 0.15	Q6DN90	*IQSEC1*
TAF1_HUMAN	11 / 10	8 / 11	212.7	5 / 8	0.43 / 0.49	P21675	*TAF1*
ZN462_HUMAN	7 / 9	6 / 4	284.7	3 / 9	0.41 / 0.41	Q96JM2	*ZNF462*
ZBTB2_HUMAN	6 / 9	5 / 6	57.3	12 / 14	0.14 / 0.19	Q8N680	*ZBTB2*
CLSPN_HUMAN	3 / 9	2 / 8	151.1	2 / 6	0.17 / 0.14	Q9HAW4	*CLSPN*
RBBP5_HUMAN	96 / 78	18 / 24	59.1	35 / 50	0.61 / 1.10	Q15291	*RBBP5*
ASH2L_HUMAN	51 / 78	13 / 19	68.7	24 / 41	0.74 / 1.25	Q9UBL3	*ASH2L*
KMT2A_HUMAN (MLL1)	10 / 9	8 / 5	431.8	2 / 2	0.78 / 1.4	Q03164	*KMT2A*
KMT2D_HUMAN (MLL2)	19 / 14	12 / 11	593.4	3 / 3	0.63 / 1.21	O14686	*KMT2D*
KMT2C_HUMAN (MLL3)	17 / 23	10 / 17	541.4	3 / 5	0.51 / 1.10	Q8NEZ4	*KMT2C*
KMT2B_HUMAN (MLL4)	5 / 5	3 / 3	293.5	2 / 2	1.14 / 0.89	Q9UMN6	*KMT2B*
SET1A_HUMAN	43 / 51	13 / 22	186.0	10 / 17	0.75 / 1.53	O15047	*SETD1A*
HCFC1_HUMAN	44 / 56	13 / 22	208.7	8 / 13	0.92 / 1.31	P51610	*HCFC1*
CXXC1_HUMAN	14 / 22	6 / 9	75.7	11 / 17	0.64 / 1.04	Q9P0U4	*CXXC1*
KANL1_HUMAN	4 / 8	3 / 7	121.0	3 / 9	0.67 / 1.08	Q7Z3B3	*KANSL1*
RERE_HUMAN	13 / 15	8 / 10	172.4	6 / 6	0.44 / 1.31	Q9P2R6	*RERE*
HDAC1_HUMAN	17 / 23	7 / 8	55.1	16 / 17	0.75 / 0.87	Q13547	*HDAC1*
HDAC2_HUMAN	13 / 19	2 / 2	55.4	14 / 15	0.67 / 0.88	Q92769	*HDAC2*

Table S3: X-ray crystallographic data collection and refinement statistics. PDPK1 peptide (Acetyl-ARTTSQLYDAVPIQS-amidated) in complex with WDR5 (22-334). Related to Figure 5.

Data collection		
Space group		$P2_1$
Cell dimensions		
	a, *b*, *c* (Å)	54.52, 47.23, 118.97
	α, β, γ (˚)	90.00, 90.92, 90.00
Resolution (Å)		2.7 (2.7-2.75)[a]
Rsym or Rmerge		0.072/0.063 (0.208/0.209)
I / σI		15.11 (3.21)
Completeness (%)		93.3 (86.2)
Redundancy		2.9 (2.2)
Structure Refinement		
Resolution (Å)		2.71-30.0
No. Reflections		15684
Rwork / Rfree		0.22/0.25
No. atoms		
	Protein	4544
	Ligand	152
	Water	49
B-factors		
	Protein	40
	Ligand	48
	Water	26
RMSD		
	Bond lengths (Å)	0.004
	Bond angles (˚)	0.751
Ramachandran		
	Favored (%)	94
	Allowed (%)	5
	Disallowed (%)	0
PDB ID code		6WJQ

[a]Values in parentheses are for highest resolution shell.

Table S4: N-terminal WIN motif-containing proteins within the human proteome. Related to Figure 5.

Protein name	WIN motif(s)	WIN motif position(s)	UniProt Accession	Gene ID
A0A0A6YYL1_HUMAN	ARS	2..4	A0A0A6YYL1	100528021
ACHE_HUMAN	ARA	2..4	Q04844	1145
BCLA3_HUMAN	ARS	2..4	A2AJT9	256643
CALR3_HUMAN	ARA	2..4	Q96L12	125972
CEBOS_HUMAN	ART	2..4	A8MTT3	100505876
CEP72_HUMAN	ARA	2..4	Q9P209	55722
CU058_HUMAN	ARS	2..4	P58505	54058
CXCL2_HUMAN	ARA	2..4	P19875	2920
CYTM_HUMAN	ARS,ARA	2..4,26..28	Q15828	1474
DHB1_HUMAN	ART,ARA	2..4,50..52	P14061	3292
DIK1A_HUMAN	ARS	2..4	Q5T7M9	388650
DIK1C_HUMAN	ARA	2..4	Q0P6D2	125704
DSG2_HUMAN	ARS,ARA	2..4,748..750	Q14126	1829
EPHB3_HUMAN	ARA,ART	2..4,525..527	P54753	2049
GNA15_HUMAN	ARS,ARS	2..4,334..336	P30679	2769
GROA_HUMAN	ARA	2..4	P09341	2919
H3-2, Q5TEC6_HUMAN	ART	2..4	Q5TEC6	440686
H31_HUMAN	ART	2..4	P68431	8350
H31_HUMAN	ART	2..4	P68431	8357
H31_HUMAN	ART	2..4	P68431	8354
H31_HUMAN	ART	2..4	P68431	8356
H31_HUMAN	ART	2..4	P68431	8358
H31_HUMAN	ART	2..4	P68431	8352
H31_HUMAN	ART	2..4	P68431	8351
H31_HUMAN	ART	2..4	P68431	8353
H31_HUMAN	ART	2..4	P68431	8968
H31_HUMAN	ART	2..4	P68431	8355
H31T_HUMAN	ART	2..4	Q16695	8290
H32_HUMAN	ART	2..4	Q71DI3	653604
H32_HUMAN	ART	2..4	Q71DI3	126961
H32_HUMAN	ART	2..4	Q71DI3	333932
H33_HUMAN	ART	2..4	P84243	3020
H33_HUMAN	ART	2..4	P84243	3021
H3C_HUMAN	ART	2..4	Q6NXT2	440093
H3Y1_HUMAN	ART	2..4	P0DPK2	391769
H3Y2_HUMAN	ART	2..4	P0DPK5	340096
HELB_HUMAN	ARS,ART	2..4,883..885	Q8NG08	92797
HIPL1_HUMAN	ARA,ARA,ARA	2..4,4..6,618..620	Q96JK4	84439
IFNA7_HUMAN	ARS	2..4	P01567	3444
ITA2B_HUMAN	ARA	2..4	P08514	3674
KLK7_HUMAN	ARS	2..4	P49862	5650
LPP60_HUMAN	ARA,ARA	2..4,51..53	Q86U10	374569
LRC4B_HUMAN	ARA	2..4	Q9NT99	94030
MIA_HUMAN	ARS	2..4	Q16674	8190
NECT2_HUMAN	ARA	2..4	Q92692	5819

Protein name	WIN motif(s)	WIN motif position(s)	UniProt Accession	Gene ID
NECT3_HUMAN	ART	2..4	Q9NQS3	25945
NPB_HUMAN	ARS	2..4	Q8NG41	256933
NT5C_HUMAN	ARS	2..4	Q8TCD5	30833
PCYXL_HUMAN	ARA	2..4	Q8NBM8	78991
PDIA5_HUMAN	ARA	2..4	Q14554	10954
PDPK1_HUMAN	ART,ARA	2..4,237..239	O15530	5170
PPR3F_HUMAN	ART,ARS	2..4,606..608	Q6ZSY5	89801
PRR25_HUMAN	ART,ART,ARS	2..4,234..236,271..273	Q96S07	388199
PTPRU_HUMAN	ARA,ART	2..4,569..571	Q92729	10076
PVR_HUMAN	ARA,ARS	2..4,268..270	P15151	5817
RAMP1_HUMAN	ARA	2..4	O60894	10267
RHXF1_HUMAN	ARS	2..4	Q8NHV9	158800
SHSA8_HUMAN	ARA,ARA,ARA,ARA	2..4,122..124,293..295,344..346	B8ZZ34	440829
SPIR2_HUMAN	ARA	2..4	Q8WWL2	84501
TM221_HUMAN	ARS,ARA	2..4,176..178	A6NGB7	100130519
TSN4_HUMAN	ARA	2..4	O14817	7106
UD110_HUMAN	ARA	2..4	Q9HAW8	54575
UD17_HUMAN	ARA	2..4	Q9HAW7	54577
UD18_HUMAN	ART	2..4	Q9HAW9	54576
WBP1_HUMAN	ARA	2..4	Q96G27	23559
WDR90_HUMAN	ARA,ART,ART,ARA,ARS	2..4,124..126,345..347,429..431,696..698	Q96KV7	197335
XPP2_HUMAN	ARA,ARA	2..4,650..652	O43895	7512

Table S5: Ninety-two oppositely regulated genes. Five high-coverage, representative enriched GO categories are presented; genes present in each category are marked. These genes are from Figures S7J and S7K: decreased expression with loss of PDPK1, increased expression with loss of WDR5, and increased expression with blockade of the WIN site. Related to Figure 7.

Gene	Regulation of macromolecule metabolic process	Organelle organization	Cell cycle	Mitotic cell cycle	Chromosome segregation
ARL15					
AKAP9	x	x	x	x	
ANKRD12					
ARHGAP5					
ARL6IP1	x	x			
ASF1A	x	x			
ASPM		x	x		
ATP8A1					
BCLAF1	x				
CAPZA1		x			
CCDC88A		x			
CENPE	x	x	x	x	x
CENPF	x	x	x	x	x
CHD9		x			
CYCS	x	x			
DBF4	x		x	x	
DDR2	x				
DEK	x	x			
DEPDC1					
DLGAP5	x	x	x	x	x
DST		x			
ECT2	x		x	x	
EHBP1		x			
EIF4G2	x		x		
FMNL2		x			
FSD1L					
GABPA	x	x			
GLS					
GPBP1	x				
HIF1A	x				
HLTF	x	x			
HMMR					
HSP90AA1	x	x	x	x	
KIAA0586		x			
KIAA1551	x				
KIAA1586					
KIF20B			x		
KIF5B		x			
KITLG	x				
KTN1					

Gene	Regulation of macromolecule metabolic process	Organelle organization	Cell cycle	Mitotic cell cycle	Chromosome segregation
LCORL	x				
LMO3	x				
LPHN3					
MAPK6	x		x		
MEIS1	x				
MMP16					
NCAPG		x	x	x	x
NDC80		x	x	x	x
NIPBL	x	x	x	x	x
NPAT	x		x	x	
ODC1	x				
PAPOLA	x				
PCDH9					
PCM1		x	x	x	
PDS5B		x	x	x	x
PGRMC1					
PHIP	x	x			
PHTF2					
PIK3R3	x				
PSAT1					
PTPLB					
RAD21	x	x	x		x
RAP2A	x	x			
RB1CC1	x	x	x		
RND3		x	x		
SACS					
SCFD1		x			
SEC63					
SEMA3D					
SENP6					
SEPT7		x	x		
SGOL2		x	x	x	x
SHOC2	x				
SMARCA5	x	x			
SMC2		x	x	x	X
SMC4		x	x	x	X
SMC6		x			
STAG2		x	x		x
TBC1D4					
TMED5		x			
TOP2A	x	x	x	x	x
TTK	x	x	x	x	x
UHRF1BP1L					

Gene	Regulation of macromolecule metabolic process	Organelle organization	Cell cycle	Mitotic cell cycle	Chromosome segregation
USP1	x				
USP16	x	x	x	x	
ZEB1	x				
ZHX1	x				
ZNF146	x				
ZNF292	x				
ZNF644	x				
ZNF654	x				
ZNF92	x				

Table S6: Oligonucleotides. Related to STAR Methods

RT-qPCR primers	
CENPE_ mRNA_1	AGCTACAGGCCTACAAACCA
CENPE_ mRNA_2	TGAGCTGTCTTCTCAGATACGC
CENPF_mRNA_1	TGAGCTGGAAGTAGCACGAC
CENPF_mRNA_2	CGGCCTTGAATAGCATCTTCTG
ASPM_mRNA_1	GGAAAGATGTGGGAGAACGTC
ASPM_mRNA_2	AACATAGCCAACCCTGTGAC
SGO2_ mRNA_1	ACCCAAAAATCAGGAATAGGTGATA
SGO2_ mRNA_2	TCTGCTTGTCCGTTCTGAAG
KIF18A_ mRNA_1	GAGAGGCACATGAAGAGAAGT
KIF18A_ mRNA_2	TGTTTTCCGGACGTACACGA
KIF20B_ mRNA_1	AATGGCAGTGAAACACCCTG
KIF20B_ mRNA_2	ACATTTCACCAAGTCCTCCTCC
CCAR1_RNA_1	GGAGGCTGATGGAGAACAGGATG
CCAR1_RNA_2	AGCTCGACTTTCTAATTCTTTTCGG
TOP2A_ mRNA_1	AAGTGTCACCATTGCAGCCT
TOP2A_ mRNA_2	ACCCACATTTGCTGGGTCAC
SMC2_mRNA_1	TTGACAGAAGCTGAAGAGCGA
SMC2_mRNA_2	TTGTTCACCTTTTGCCATGC
SMC3_ mRNA_1	TGTGATTGTGGGCAGAAATGG
SMC3_ mRNA_2	CCGCTGTTCTGGACGAAGAT
SMC4_ mRNA_1	TTGAACAGCATTCCTCCTCCC
SMC4_ mRNA_2	GGAAAAGCGCTTATGGAAAGGT
RPL35_mRNA_1	AACAGCTGGACGACCTGAAG
RPL35_mRNA_2	ACTGTGAGAACACGGGCAAT
GAPDH_mRNA_1	AAGGTGAAGGTCGGAGTCAAC
GAPDH_mRNA_2	GTTGAGGTCAATGAAGGGGTC
RPL14_mRNA_1	GTCTCCTTTGGACCTCATGC
RPL14_mRNA_2	ATGGCCTGTCTCCTCACTTG
Run-On CENPE For	TGCGTATGTGTGTTTTGTTT
Run-On CENPE Rev	TGATCTTCTGAACCCATCAT
Run-On CENPF For	ACTGGTTTTAGCAGCCAAACT
Run-On CENPF Rev	ATCTTTGGCCAGACACACCC
Run-On ASPM For	ATAATGTATTGTTTTGATTATAGCC
Run-On ASPM Rev	ATCTCTCTTACTCGGCCTTC
Run-On KIF18A For	GGTGAGAAGTCATTGGAGAC
Run-On KIF18A Rev	TGATACGTTCATCAAAAGCA
Run-On TOP2A For	GGTTAACTGCCTTTGATGAGCTT
Run-On TOP2A Rev	ACATATTTTGCTCCGCCCAG
Run-On KIF20B For	AGGGAAGTAGTGGGCTAGACT
Run-On KIF20B Rev	GTCGAGGTACTCCCTCTTGAT
Run-On SGO2 For	TTTCTTCGCCTAAAGCTAAA
Run-On SGO2 Rev	GCTTCTATAATAATGCAGCTAAAA
Run-On RPL35 For	CTGAGGCACACTCTCTCTTG
Run-On RPL35 Rev	GTCGTCCAGCTGTTTCAG
Run-On RPS24 For	CCTGGATGTACTCTTTTCTCA
Run-On RPS24 Rev	ATTCTGTTCTTGCGTTCCT
Run-On ACTB For	AGCTCATTGTAGAAGGTGTGG
Run-On ACTB Rev	GGCATGGGTCAGAAGGATTC